FLUID FLOW IN POROUS MEDIA: NMR IMAGING AND NUMERICAL SIMULATION

Margaret S. Edie, John F. Olson, Daniel R. Burns, and M. Nafi Toksöz

Earth Resources Laboratory
Department of Earth, Atmospheric, and Planetary Sciences
Massachusetts Institute of Technology
Cambridge, MA 02139

ABSTRACT

We use nuclear magnetic resonance (NMR) imaging to obtain a three-dimensional image of the pore structure in a limestone core, 4.5 mm in diameter and 10 mm in length, with a resolution of 40 μm. This image is converted into boundary conditions for simulation of fluid flow through the rock using the lattice gas method. The computed permeability is several orders of magnitude lower than the laboratory measured permeability, most likely a result of the image resolution being too coarse to resolve the smaller pore throats, which are believed to be significant for flow in this sample.

INTRODUCTION

How does fluid flow through a complex porous medium? This is a question that has been studied by hydrologists monitoring groundwater, chemists tracking soil contamination, petroleum geologists trying to extract more oil from reservoirs, and geophysicists studying the flow of mantle melt through the Earth's crust. Despite many years of research, it remains a difficult question to answer because the medium is opaque and the process cannot be directly observed.

Laboratory and field experiments have been designed to try to understand how fluid moves through a matrix of rock or soil. Bulk parameters such as permeability, conductivity, and average velocity can be measured, but we can only guess at the details of the motion taking place inside the sample. However, the development of computer-simulated fluid dynamics has created a setting where flow at the microscopic level can be explored virtually. To perform such simulations using realistic models of pore space, and

therefore relate simulations to laboratory measurements on real rocks, it is necessary to obtain detailed digital images of the pore geometry of geologic samples.

Gathering three-dimensional images of this kind is a difficult task and the techniques that have been tried have had mixed results. The methods that yield very high resolution are limited by imaging only in two dimensions or only very small volumes, and it is usually necessary to destroy the sample in the process. However, nuclear magnetic resonance (NMR) is a noninvasive and nondestructive technique that has been used for years in the biological sciences for imaging human organs and has recently been applied to the study of porous media in geologic environments. Attempts have been made to image the pore space of limestones (Gleeson *et al.*, 1993) and characterize oil fields (Nurmi, 1997), as well as to examine flow through porous media (Guilfoyle *et al.*, 1992).

The work presented in this paper is an attempt to bring together NMR imaging and numerical simulation of fluid flow to better understand the microscopic flow properties. Included is a summary of previous work done in both imaging of pore space and computer-simulated flow through porous media, as well as a brief description of NMR imaging. The NMR imaging methods used to obtain a three-dimensional image of the pore structure in a limestone sample are presented. This image is converted into boundary conditions for simulating fluid flow using the lattice gas method. The results of the simulation are discussed and calculated permeability is compared with the laboratory measured permeability.

BACKGROUND

Pore Geometry Imaging

It is necessary to have detailed pore structure information in order to effectively model the processes taking place in the pore space of our sample. One way of doing this is to take thin slices of the rock, obtain two-dimensional SEM images and stack the images together. However, interpolation between stacked slices leads to errors in the image and portions of the sample are lost when the rock is cut and polished to gather the SEM image. Another possible method is to push a mold-forming liquid through the rock, wait for it to harden and then dissolve the rock around it. This method is not very practical for obtaining a digitized image, since there is no simple way to transfer the pore structure in a format that can be analyzed by a computer. Also, it is likely that resin will only enter areas of connected porosity, which means that some of the pore space will not be imaged.

More recent methods include laser-scanning confocal microscopy (LSCM), synchrotron computed microtomography, and nuclear magnetic resonance imaging. LSCM can produce very detailed, three-dimensional images of pore space, but the vertical extent is only a few hundred micrometers below the surface of the sample (Fredrich *et al.*, 1995). To probe deeper into the sample, it would be necessary to cut the rock. Similarly, with synchrotron microtomography, it is only possible to image a sample with dimensions of one or two millimeters (Spanne *et al.*, 1994). Lastly, there is NMR, which can be done

in three dimensions for a variety of sample sizes without destroying the sample.

Nuclear Magnetic Resonance Imaging

Most elements have at least one isotope with a nucleus that possesses a nonzero spin angular momentum, giving them a magnetic moment. A nucleus with spin quantum number of $1/2$ is often used in NMR because it behaves like a magnetic dipole. Hydrogen is such an element which is popular for use in NMR experiments because of its natural abundance.

If a sample of water is placed in a static magnetic field, quantum mechanics requires that the spins of the hydrogen nucleus align either with the field or against it. Due to the uncertainty principle, the spins will not be parallel to the field; instead they will reside in one of the two cones offset from the field direction (Figure 1). The two different cones represent two energy states. Moving between these states requires an absorption or release of energy, and it is this emitted energy which results in nuclear magnetic resonance.

Consider the net magnetic moment for the sample (Figure 2). If the net moment is perturbed from this state, it will return to the equilibrium by growing in the z-direction while precessing about the z-axis. The frequency, ω, of this rotation, often called the Larmor frequency, is proportional to the strength of the magnetic field, B, by the relation:

$$\omega = \gamma B$$

where γ, the gyromagnetic ratio, is an intrinsic property of the nucleus.

To push the net moment out of alignment, a wire is coiled around the sample such that radio frequency (RF) radiation emitted from it produces a rotating magnetic field, which is perpendicular to the original field. If the rotating magnetic field is at the Larmor frequency, it has just the right amount of energy to cause individual moments to jump from one energy state to another. This causes the net moment to rotate away from the axis of the magnetic field B and into the x-y plane (Figure 3). When the rotating magnetic field is turned off, the system will return to equilibrium.

The return to equilibrium for the net moment is represented by two times. The spin-lattice relaxation time, T1, represents the time it takes for the net magnetic moment to grow along the z-axis (Figure 4). The equation describing the magnitude of the net magnetic moment, M_z, along z at any time, t, is

$$M_z = M_0(1 - e^{t/T1})$$

where M_0 is the initial magnitude of M_z. The second kind of relaxation occurs because each individual moment will be rotating in the x-y plane at a slightly different frequency due to magnetic field inhomogeneities. Therefore, some spins will rotate faster than others, and eventually they will cancel out. The spin-spin relaxation time, T2, represents the time it takes for this to occur. The oscillation of the magnetic moment in the x-y

plane produces an oscillating electrical signal at the Larmor frequency that decays over time in the coils around the sample. The decay is exponential with time, t, and is represented by $e^{-t/T2}$ (Figure 5). This signal is called a free induction decay (FID).

If a magnetic field gradient is applied evenly across the sample, the Larmor frequency will vary across the sample. By applying the RF radiation in a short pulse, recording the FID and then repeating, FID's are obtained for all locations in the sample. This sequence of events is called a pulse sequence. Using a Fourier transformation, these signals are converted into signal intensities at varying frequencies. Because of the gradient, certain frequencies correspond to specific locations in the sample and the signal intensities can be mapped out. This yields an image of the sample.

This explanation is a limited summary of an enormous field of study. More detail on the subject can be found in many introductory books, such as Fukushima and Roeder (1981) and Slichter (1990).

NMR in Geoscience

To image pore space in rock using NMR microscopy, the rock must be saturated with a fluid that possesses a nuclear magnetic moment. Typically water is used since hydrogen yields a strong signal and is abundant and inexpensive. One problem with using NMR to image pore space is that unless the porosity is very large, the amount of water present in a saturated porous rock is small, which results in weak signal intensity. Gleeson *et al.* (1993) used NMR to image pore space in rocks with relatively large pores, such as limestones. By taking 3D slices of the rock with NMR, the type of pore space could be classified, although the study was limited to samples with pore space larger than 80 μm, the resolution limit of the technology at the time. Recently, sandstone samples were imaged at a resolution of 11.5 μm, the highest resolution achieved so far with granular materials (Doughty and Tomatsa, 1998).

In addition to imaging, NMR can be used to obtain fluid velocity distributions across a sample. This technique has been applied to many types of samples including peat (D. Caputo, pers. comm.) and sandstone (Tessier and Packer, 1998). Further, NMR can be used to map the location and density of different chemical compounds since they have different T1 relaxation times. The pulse sequence can be adjusted so that the signal is recorded from only one chemical species. Chen *et al.* (1988) used this technique to image oil penetration of a water saturated rock sample.

More commonly, NMR is used in borehole logging to characterize petroleum reservoirs (Nurmi, 1997). To do this, a magnet is placed down a well and the magnetic field penetrates into the reservoir. This is not an imaging technique, but rather a way to obtain useful information such as pore size distribution and effective porosity from the relaxation times, T1 and T2. This data, combined with resistivity and seismic data, can be used to construct a more complete view of the reservoir (Sklar, 1997).

Fluid Flow Experiments

Data collected from field experiments to characterize reservoirs are mainly from remote sensing techniques, such as electrical resistivity or seismic surveys because it is not practical to drill hundreds of wells to investigate a given area. Being able to extract information about the fluid type, fluid volume and permeability from these data is difficult without having information at the microscopic level. For example, understanding how fluid dissipates the energy of a seismic wave traveling through it may make it possible to directly relate seismic attenuation to fluid properties.

One method to examine microscopic flow is to create a synthetic model of the pore space from clear epoxy and push dyed fluid through the synthetic rock so that flow can be directly observed (Brown *et al.,* 1998). Another method is to study thin sections from the medium and create relationships between the fractal dimension of the pores and permeability, porosity and conductivity (Thompson, 1991). A third method is to use NMR to obtain average velocity fields of the fluid as it moves through a porous rock (Tessier and Packer, 1998). Finally, computer simulations recently have been shown to compare well with laboratory experiments and, therefore, may be useful for studying microscopic flow (Auzerais *et al.,* 1996).

Fluid Flow Simulations

There are two main ways to do computer simulations of fluid flow—the finite difference or finite element method and the lattice-gas method. The finite difference method has been used extensively and can be applied to problems such as modeling the flow of air around a plane in flight and the circulation of water in an ocean basin (Versteeg and Malalasekera, 1995). The basic method is to numerically model the Navier-Stokes equations:

$$\frac{\partial u}{\partial t} + u \bullet \nabla u = -\frac{1}{\rho}\nabla p + \upsilon \nabla^2 u$$

$$\nabla \bullet u = 0.$$

The lattice-gas method models the fluid movement as the movement of many small particles whose average motion results in these equations. The particles are confined to the nodes of a lattice and move from node to node in regular time steps. All the particles have the same speed and mass, and there are a finite number of velocities that the particles can possess, determined by the lattice. For example, in two dimensions, a hexagonal lattice is used and only six velocities are possible. The model steps through time, and at each time step the particles jump to a new node and then collide (Figure 6), conserving mass and momentum (Rothman and Zaleski, 1997).

Olson (1995) developed a three-dimensional fluid simulation program that uses the lattice-gas method to simulate fluid flow based largely on the code written by Somers and Rem (1991, cited in Olson, 1995), which uses collision rules created by Westland (1991,

cited in Olson, 1995). The model uses a "face-centered hypercubic" lattice (Figure 7) where each node is connected to 24 other nodes. Therefore, a set of only 24 velocities can be used to model fluid flow. The particles move around on the lattice as described earlier, except at the boundaries. When a particle hits a wall, it bounces off with a velocity exactly opposite its precollision velocity. This results in average velocities being zero near the walls, in other words, a no-slip boundary condition.

The unique piece of this model is that it has been coded to exert pressure forces on the particles instead of body forces (J. Olson, pers. comm.). To exert a body force, nodes are selected at random and the velocities of the particles at each node are changed so that the net momentum at each node is as large as possible in the direction of the force. But in order to study the effects of seismic wave propagation, it was necessary to set up a pressure force instead. Olson does this by randomly choosing particles to remove from one side of the sample and locating them on the opposite side. This sets up a density gradient that drives the particles across the sample

METHODS

Imaging

The pore space of the rock was imaged using Nuclear Magnetic Resonance. The superconducting magnet has a strength of 3 Tesla and a horizontal 15 cm bore. The gradient power was set to 35 Gauss/cm. A Bruker Instruments AMX300 spectrometer was used for processing.

The rock sample is a calcarenite with a total porosity of 23%. A core 4.5 mm in diameter and 10 mm long was cut. For imaging it was placed in a 5 mm NMR glass sample tube and saturated with deionized water.

The imaging sequence used was a 3D spin-echo pulse sequence (Figure 8). The $\pi/2$ pulse is a sinc pulse ($\sin x/x$) which selects a smaller range of frequencies to excite along the z-axis. Gradients are applied along all three directions to spatially encode the spins. The π pulse refocuses the spins so that the echo can be recorded. Fourier transform of the FID is performed producing the reconstruction of the rock by ^{1}H intensity in each pixel. The image is $128 \times 128 \times 64$ pixels, which results in a resolution of 40 micrometers in all three directions. In order to increase signal to noise, the image is averaged over 12 scans.

At 40 μm resolution, each pixel contains both rock and pore space with the signal intensity reflecting how much pore space is present. In order to use the image as boundary conditions for the numerical simulation, the signal intensity must be converted into a binary matrix where each pixel of the image represents one entry in the matrix. Processing an image of rock structure in order to derive information about pore volume is a complex problem. Therefore, a simple method for converting the image to a binary matrix was chosen. A threshold level of intensity was determined below which the pixel was considered to be rock, and above pore space. The threshold level was chosen such that the calculated porosity matched the laboratory measured porosity, a method

similar to that of Spanne *et al.* (1994) who converted their tomographic data to binary pore geometry.

Simulation

To perform the simulation, the binary matrix of pore geometry was used to establish the boundary conditions by mapping rock locations to wall nodes and pore locations to fluid nodes. In the fluid nodes, lattice gas particles were distributed at random. A section of the rock was extracted for the simulation. A pressure force was applied across this section by moving ten particles per time step from the end of the rock sample to the front, creating a density gradient that drove flow through the sample.

Once steady state was reached, the density, mass and momentum were averaged over 30,000 time steps. The pressure was computed from the density. The pressure gradient across the sample was calculated by a linear, least squares fit to the data. Using this gradient, the permeability was calculated using Darcy's Law:

$$\frac{Q}{A} = \frac{k}{\mu}\frac{\Delta p}{\Delta x}$$

where Q is the volume flux, μ is the viscosity, A is the cross-sectional area of the sample, $\Delta p/\Delta x$ is the pressure gradient, and k is the permeability.

RESULTS

Imaging

Figure 9 shows the image of the rock sample (details of the image processing can be found in the appendix). The resolution is 40 micrometers in all three directions. Despite the limited resolution, some of the structure in the rock is revealed. The signal intensity, which is correlated to spin density and thus to percent water content, is plotted on a continuous color scale. The red, yellow, and green areas represent high signal intensity and the dark blue and purple areas low signal intensity. It looks as though there is layering in this sample. There are two bands of low signal intensity clearly visible. Looking at the porosity across the sample (Figure 13), this corresponds well with the dips in porosity at slice 22 and slice 35. This banding cannot be explained as an imaging effect because the energy put into the spins is uniform across the middle of the sample.

Figure 10 is a slice through the rock. The crescent of red around the edge of the slice is due to the water surrounding the rock sample. The dark blue outside the circle is background noise. The red and yellow areas inside the rock are pores. The light blue areas are pixels where both water and rock are present. Figure 11 is the image after the threshold is applied. The black areas are now considered pore space. Much of the light blue areas have become rock, which means that there is more pore information at a scale finer than the resolution of the image.

The smaller pore space can be seen in Figure 12, which is a scanning electron microscope (SEM) image of the rock made at New England Research Laboratory, Inc.

Comparing this thin slice from the same rock sample with the NMR image shows that the NMR image does not reproduce all the detail of the SEM image. However, the NMR image captures most of the larger pore structures.

Figure 13 is a plot of calculated porosity in each slice of the rock. The range in porosity is large, 0.10 to 0.35, which is not surprising considering that the sample is very heterogeneous. There is a section of the sample with 10% porosity which is about 200 μm wide. This section most likely controls the permeability for this sample because the same flux must pass through a smaller area.

Simulation

A section of the rock, 70 × 70 × 50 pixels, was used for simulation. Several different sections were tested before one was located where there was a connection across the whole sample. The simulation would not run at high flow rates. It was necessary to lower the mass flux several times before a successful simulation of flow was possible, which suggests that the connectivity in the image of the sample is very low.

The profiles of mass flux through the sample are shown in Figure 14. The simulation results are averaged over 30,000 time steps. The pressure was forced in the z-direction, through the slices. We know that steady state has been reached because the mass flux in the directions perpendicular to the forcing are small and centered around zero, while the mass flux in the direction of forcing is large and constant across the sample.

Figure 15 shows the pressure across the sample. Pressure is computed from the density treating the particles as an ideal gas. This relationship is:

$$P = c_s^2 \bullet \rho$$

where P is the pressure, c_s is the speed of sound which is $1/\sqrt{2}$ in lattice units, and ρ is the density. The pressure gradient is approximately linear, which is what is expected for constant flow through a rock at steady state. Using the pressure gradient, and knowing the volume flux, viscosity and area of the sample which is set in the simulation, Darcy's Law is used to calculate the permeability. The calculated permeability ranged between 0.2 and 1.8 μD. This is extremely low compared with the permeability measured in the lab on a core sample 46.5 mm long and 38 mm in diameter, which was between 250 and 400 mD.

DISCUSSION

There are several explanations for the large difference between the measured and calculated permeabilities. The most likely is the resolution of the imaging. There are small pores that are seen in the SEM image but not in the NMR images. It is possible that smaller pore throats, which are not being imaged by NMR, connect the large pores seen in the images. These smaller pores may contribute heavily to the greater connectivity in the rock as evidenced by the high laboratory measured permeability values.

There are several problems with NMR imaging at higher resolution because the number of pixels and the magnetic gradients must be increased. On the magnet used for this work, the number of pixels can be doubled, but due to computational limitations, files larger than this cannot be obtained. There is also a problem with the signal strength at higher resolution. Approximately only one in every million spins resonates. Therefore, for a small pixel volume, a very small number of spins will resonate, producing a low signal.

To maximize the signal to noise ratio, it is necessary to do two things. First, the time between pulse sequences can be increased. The relaxation of the spins is logarithmic with time and, therefore, choosing the time between pulsing to be 1–2 seconds is satisfactory. To be assured that you get the maximum signal, it is necessary to wait longer. Waiting assures that all of the spins return to equilibrium before the RF pulse is applied again. The other way to increase the signal to noise ratio is to increase the number of images that are averaged together. The noise should be random and as the signal is added to itself, it should show up more prominently than the noise. The time between pulses and the number of averages are simple to change, but it makes running the image time intensive. It could take more than 10 days to obtain this kind of image.

It should be possible to double the number of pixels and improve the resolution to 20 μm. Increasing resolution beyond this may be difficult with the present computing capacity. Doughty and Tomutsa (1998) were able to obtain images with a resolution of 11.5 μum. They used a specially designed magnet with a very strong magnetic field to do this work. M.I.T. has magnets with stronger fields but they require a sample size of 1 mm. A rock sample only 1 mm across will contain only two or three grains across and will not be very helpful in determining permeability. Such a sample would not contain any of the structure of the larger bulk sample.

The other possible explanation for the permeability difference is that the calcarenite sample is very heterogeneous. When selecting a small core from the sample to image, it is possible that a section of the rock with very low permeability was taken. Several things could be done in the future to correct for this problem. One is to choose a fairly homogeneous rock sample so that we are assured that a small section taken from the larger sample will be representative. Also, it would be informative to gather pore size distribution information about the rock by analyzing thin sections. This could be compared against the pore sizes that are being seen in the NMR images.

CONCLUSIONS

In this work, we have combined two powerful techniques for studying flow in porous rock: NMR imaging and fluid simulation by the lattice gas method. NMR images of a three-dimensional pore structure at 40 μm resolution were acquired and used as boundary conditions in simulations of fluid flow. However, the calculated and measured permeabilities were significantly different; this difference was not surprising because it could be seen from comparing the SEM and NMR images that much of the small pore

space was not resolved.

There is much more work that can be done on this problem. The first issue to address is the image resolution. Imaging at a scale of 10 μm is possible and most of the pore structure responsible for flow should be seen at this resolution. Another issue that was not examined in this work is the best method to extract porosity information from an image. A lot of work has been done in this area, and it is likely that there are better methods than the one used here. It would be useful to incorporate statistical information about the rock, such as grain size and pore size distributions, in the conversion of the NMR image to the digitized image used in the simulation.

Finally, imaging of flow with NMR is possible and produces accurate flow fields from laboratory experiments. Even if the computed and measured permeabilities are similar, it is still unclear whether or not the flow fields produced by the simulation represent the actual processes taking place in a rock sample as fluid moves through it. Comparing the results of NMR flow experiments with the simulation might be the best way to understand how closely this simulation reproduces the real physics taking place inside the rock.

ACKNOWLEDGMENTS

This work was supported by the Borehole Acoustics and Logging/Reservoir Delineation Consortia at the Massachusetts Institute of Technology, and by the Saudi Arabian Oil Company.

REFERENCES

Auzerais, F., Dunsmuir, J., Ferreol, B., Martys, N., Olson, J., Ramakrishnan, T., Rothman, D., and Schwartz, L., Transport in sandstone: A study on three dimensional microtomography, *Geophys. Res. Lett., 23,* 705–708, 1996.

Brown, S., Caprihan, A., and Hardy, R., Experimental observation of fluid flow channels in a single fracture, *J. Geophys. Res., 103*, 5125–5132, 1998.

Chen, J., Dian, M., Patz, S., and Schwartz, L., Magnetic resonance imaging of immiscible-fluid displacement in porous media, *Phys. Rev. Lett., 61*, 1489–1492, 1988.

Doughty, D. and Tomatsa, L., Pore structure and connectivity of porous rock by high resolution NMR microscopy, in *Spatially Resolved Magnetic Resonance,* Wiley-Vch Pub., 1998.

Fredrich, J., Menendez, B., and Wong, T., Imaging pore structure in geomaterials, *Science, 268*, 276–279, 1995.

Fukushima, E. and Roeder, S., *Experimental Pulse NMR: A Nuts and Bolts Approach,* Addison-Wesley Pub., 1981.

Gleeson, J., Woessner, D., and Jordan, C., NMR imaging of pore structures in limestones, *SPE Formation Evaluation, 8*, 123–127, 1993.

Guilfoyle, D., Mansfield, P., and Packer, K., Fluid flow measurement in porous media by echo-planar imaging, *J. Mag. Res., 97,* 342–358, 1992.

Nurmi, R., Carbonate reservoir characterization with integration of new technology reveals insight into old giants, *AAPG Bulletin, 81,* 1584–1585, 1997.

Olson, J., Two-fluid flow in sedimentary rock: Complexity, transport and simulation, Ph.D. Thesis, MIT, 1995.

Rothman, D. and Zaleski, S., *Lattice-Gas Cellular Automata: Simple Models of Complex Hydrodynamics,* Cambridge University Press, 1997.

Sklar, H., Nuclear magnetic resonance logging, M.S. Thesis, MIT, 1997.

Slichter, C., *Principles of Magnetic Resonance,* Springer-Verlag, 1990.

Somers, J. and Rem, P., Analysis of surface tension in two-phase lattice gasses, *Physica D, 47,* 39–46, 1991.

Spanne, P., Thovert, J, Jacquin, C., Lindquist, W., Jones, K., and Adler, P., Synchrotron computed microtomography of porous media: Topology and transport, *Phys. Rev. Lett., 73,* 1994.

Tessier, J. and Packer, K., The characterization of multiphase fluid transport in a porous solid by pulsed gradient stimulated echo nuclear magnetic resonance, *Phys. Fluids,* 75–85, 1998.

Versteeg, H. and Malalasekera, W., An introduction to computational fluid dynamics: The finite volume method, *Longman Scientific & Technical,* 1995.

Westland, G., Optimizing a reduced collision table for the FCHC-lattice gas automaton, Master's thesis, State University of Utrecht, 1991.

APPENDIX

IMAGE PROCESSING

The image quality varied across the slices of the sample. At the ends, this is due to the sinc pulse. If you look at the Fourier transform of the sinc pulse, it has the shape of a box car. Ideally, this is the energy that is applied along the sample, such that the middle section of the sample receives equal amounts of energy and the rest receives none. The true pulse is flat across the top with gradually decreasing edges to zero. Therefore, the ends of the imaged section have a lower signal intensity because they receive less energy than the middle.

The reason the middle slices have such low signal intensity is due to a scaling problem. The power was too high and produced the anomalous red spot in the center of the image because in the Fourier transform signal at the ends spills over and gets folded back into the center of the image (Figure 16). [Note: The image was off-center due to incorrect phasing during the NMR imaging. This does not affect image quality. The image is a $128 \times 128 \times 64$ matrix of numbers and was translated to the left by moving the first 20 columns of each slice to the other side.] The signal in these pixels is so much higher than the normal signal that the signal in the rest of the slice and the noise appear to be about the same (Figure 7). The outlying values were replaced with the average value around the bright spot.

Each slice was scaled to the rest of the slices by multiplying by a constant. The scaling constant was chosen for each slice so that the signal intensity of the water surrounding the rock was similar (Figure 18). This is a reasonable choice since the signal from a pixel of water should be a constant. However, the noise in slices with lower signal intensity became much higher than the noise in the rest of the slices. In the future, this can be avoided by optimizing the pulse sequence to avoid the anomalous features and leaving the end slices out of the simulation.

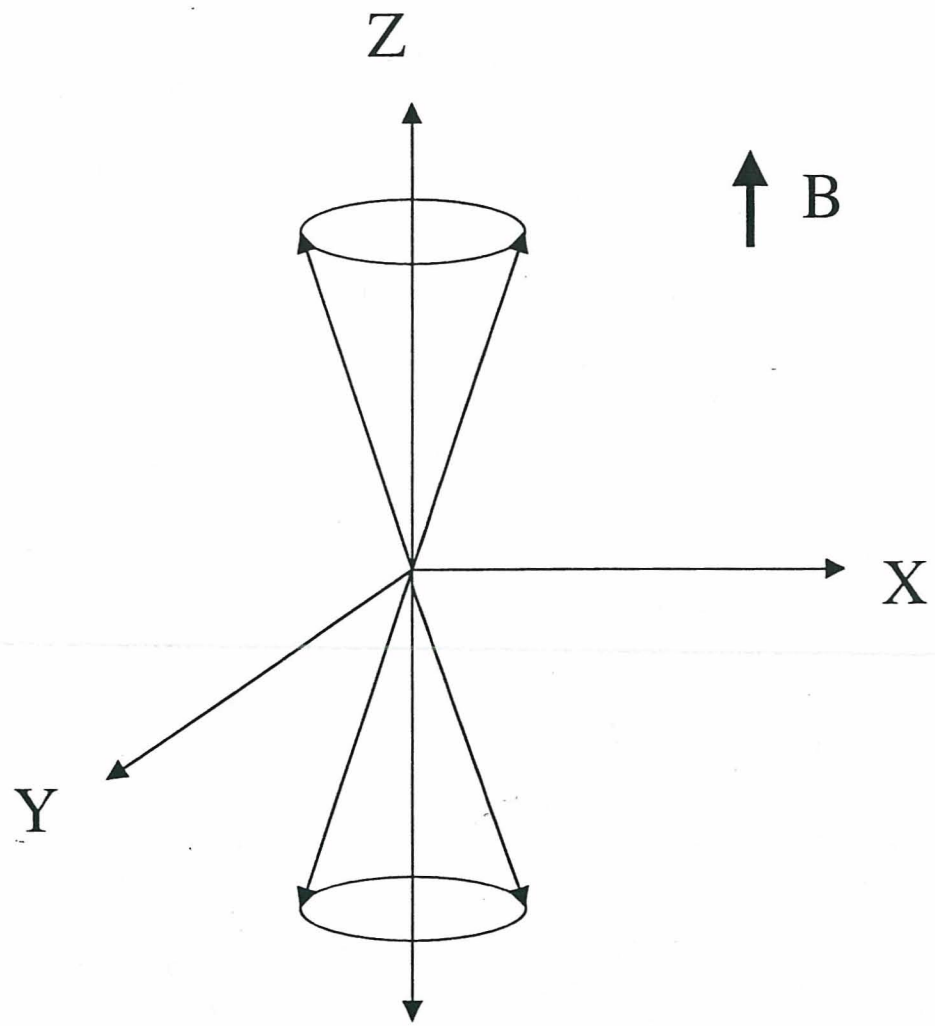

Figure 1: The individual spins are located in these two cones, which represent the two energy states.

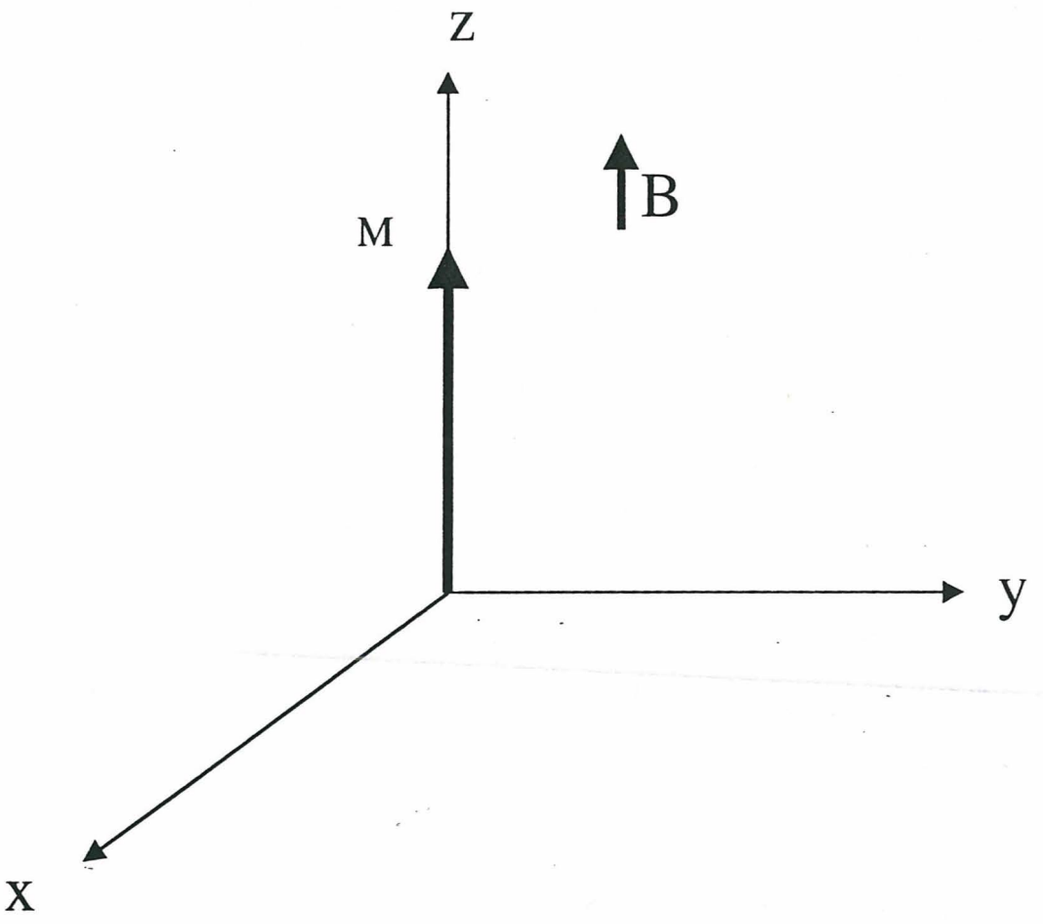

Figure 2: Net magnetic moment vector, M, in a static magnetic field, B.

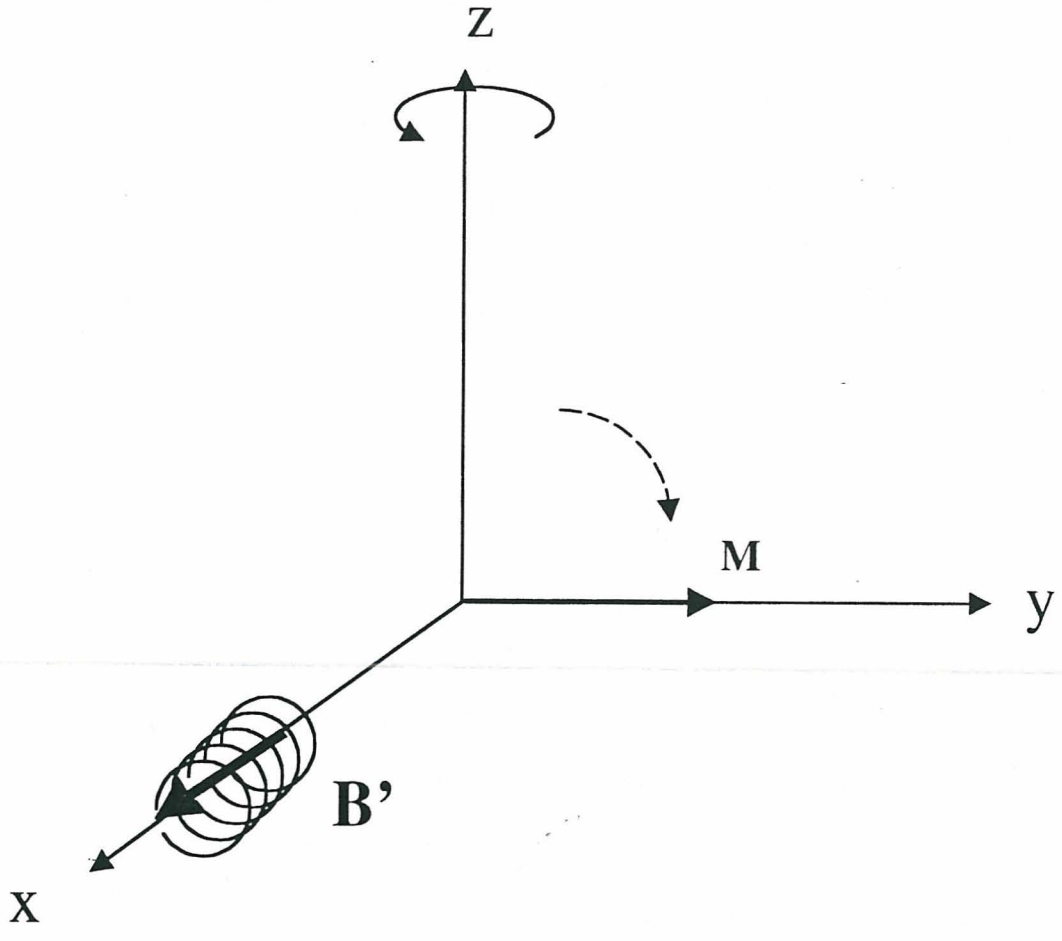

Figure 3: In a rotating reference frame, an oscillating magnetic field, B', is applied and the magnetic moment vector, M, flips into the x-y plane.

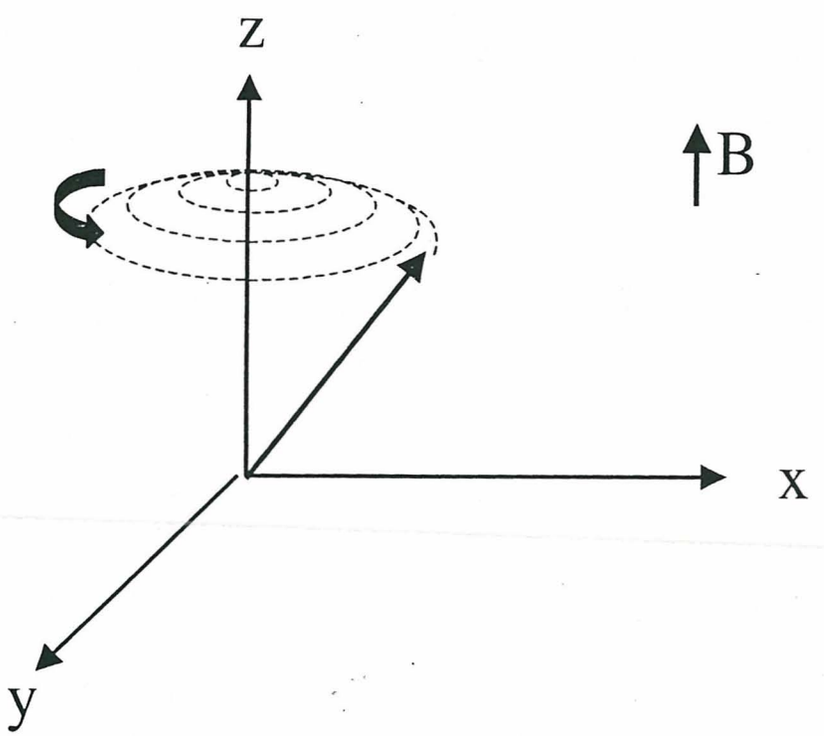

Figure 4: The net magnetic moment, M, precessing about the static magnetic field, B.

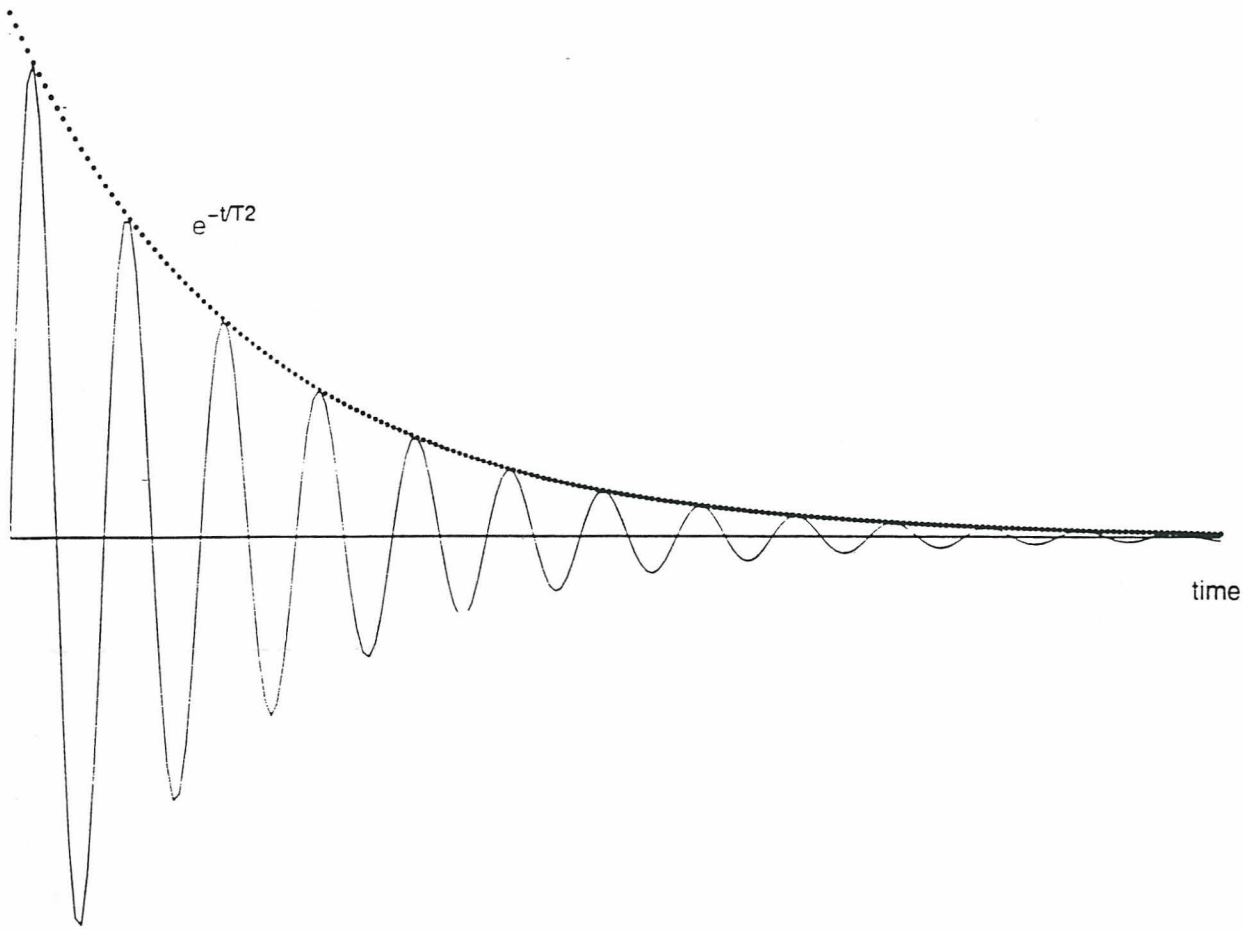

Figure 5: The signal intensity decays exponentially with time as the individual magnetic moments oscillate around the z-axis. The decay rate is determined by the $T2$ relaxation time.

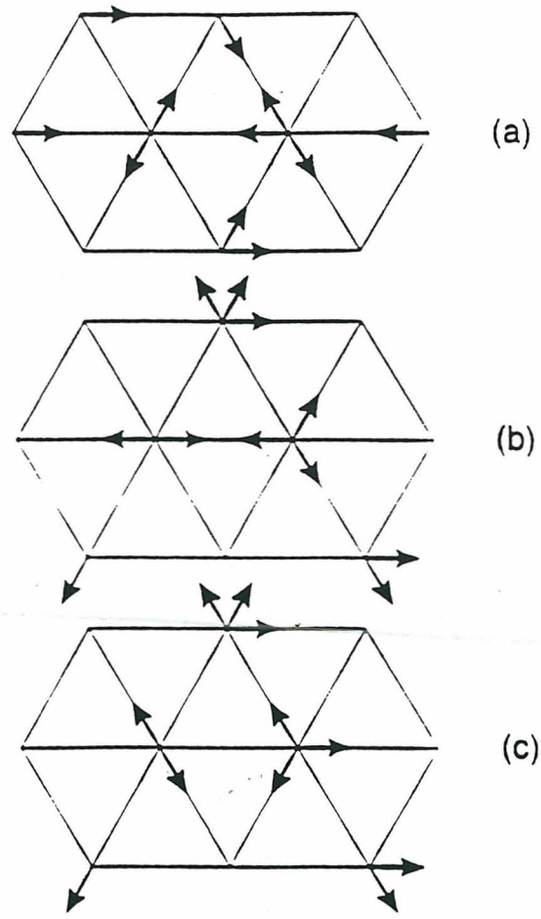

Figure 6: The motion of lattice gas particles on the two-dimensional hexagonal lattice. The original state is seen in (a). At the next time step, the particles shift to a new node (b), and the particles are rearranged obeying the rules of collision (c). (Figure from Rothman and Zaleski, 1997.)

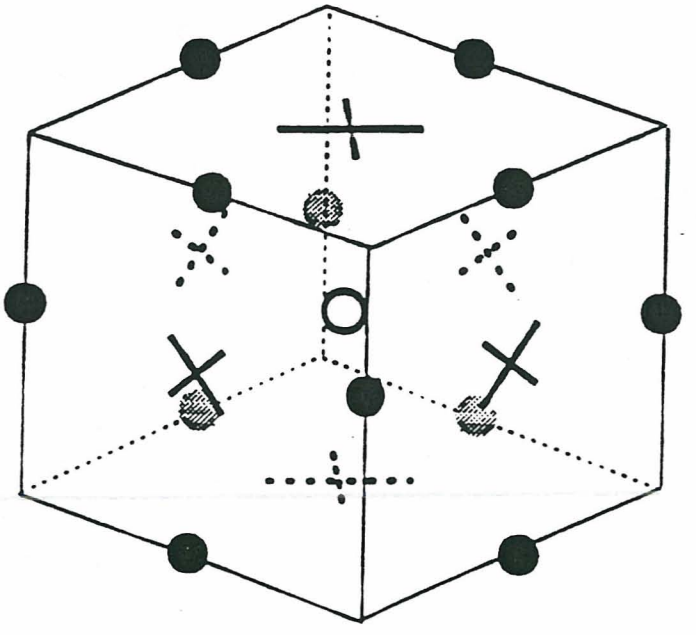

Figure 7: The "face-centered hypercubic" lattice is used in three-dimensional lattice gas simulation models. The open circle is the node at the center of the box and the filled circles are its neighboring nodes. (Figure from Olson, 1995.)

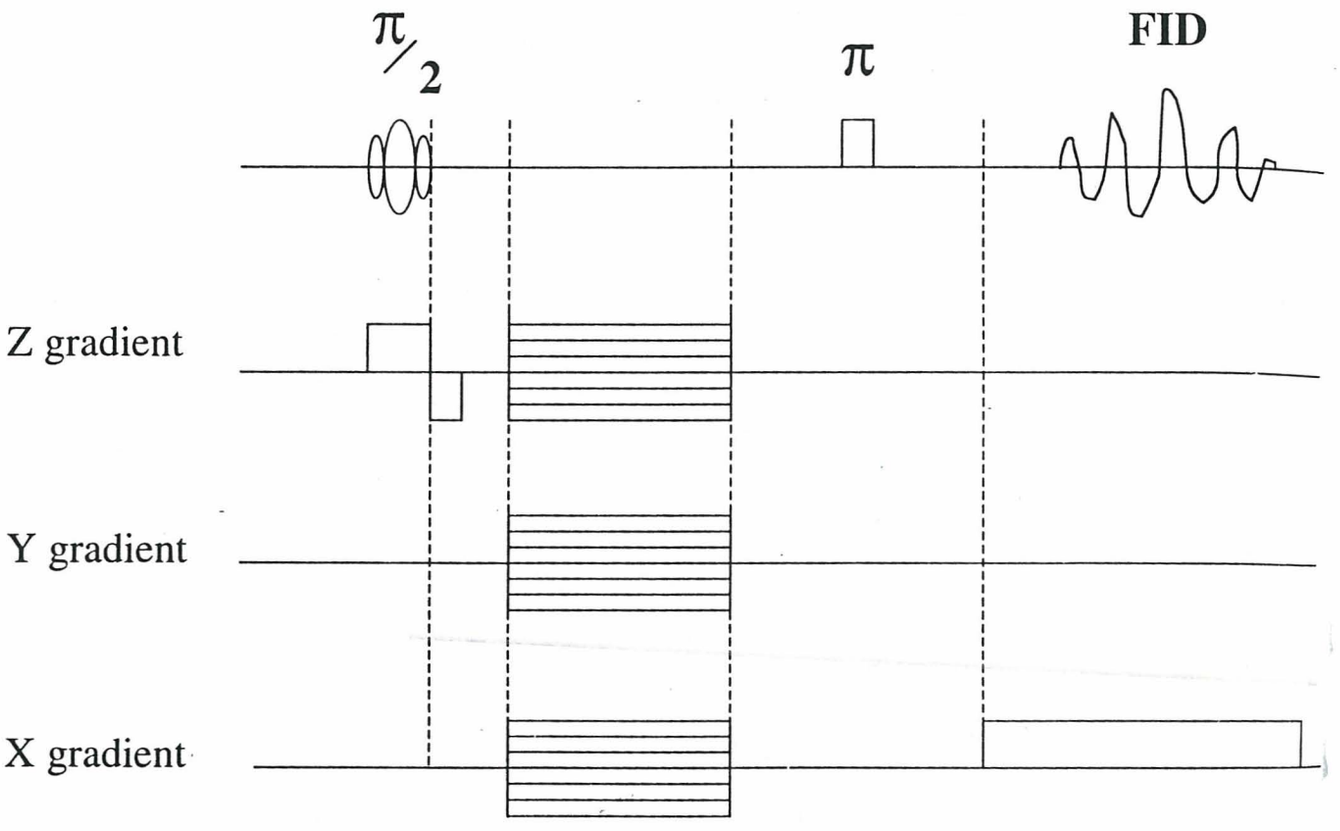

Figure 8: The spin-echo pulse sequence with a sinc $\pi/2$ pulse for slice selection. The gradients are cycled after the initial pulse for three-dimensional imaging.

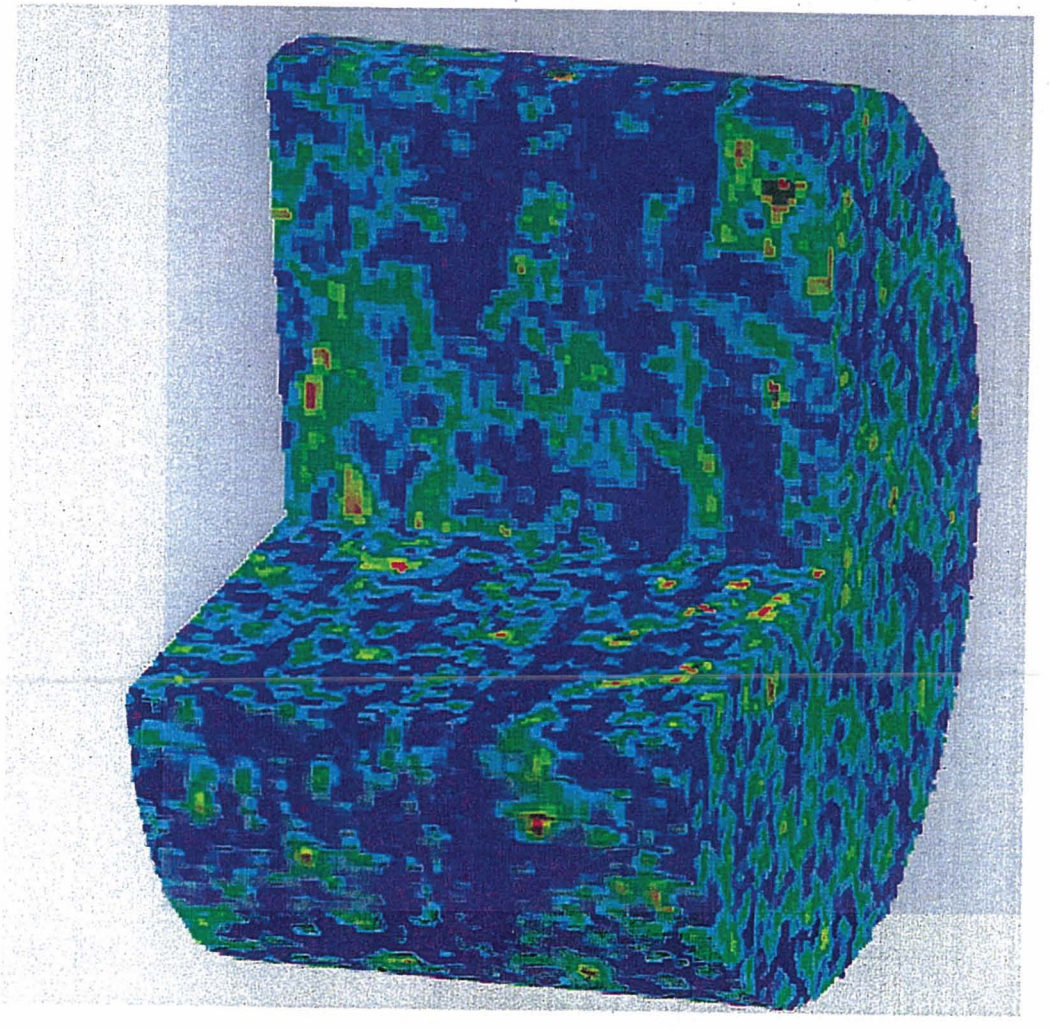

Figure 9: A three-dimensional image of the calcarenite sample from NMR imaging. The red, yellow, and green areas represent high signal intensity, and the blue and purple areas represent low signal intensity. The signal intensity indicates the amount of water present in a pixel so that areas of high signal intensity are considered pore space.

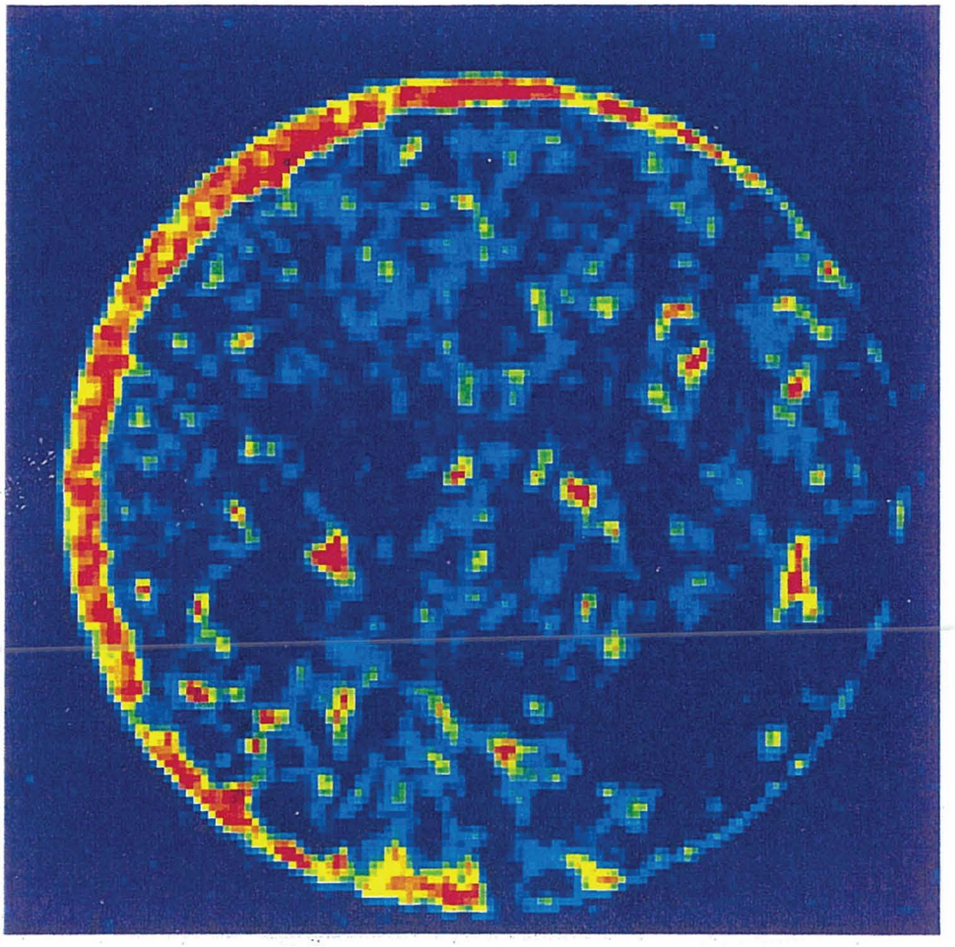

Figure 10: A slice through the sample. The red and yellow areas represent water filled areas, and the dark blue represents the rock. The blue area around the circle is noise.

Figure 11: A slice through the binary image that is used in the simulation. fig An image of the calcarenite taken with a scanning electron microscope. The distance across the bottom of the image is 2.64 mm. The blue areas show pore spaces.

Figure 12: An image of the calcarenite taken with a scanning electron microscope. The distance across the bottom of the image is 2.64 mm. The blue areas show pore spaces.

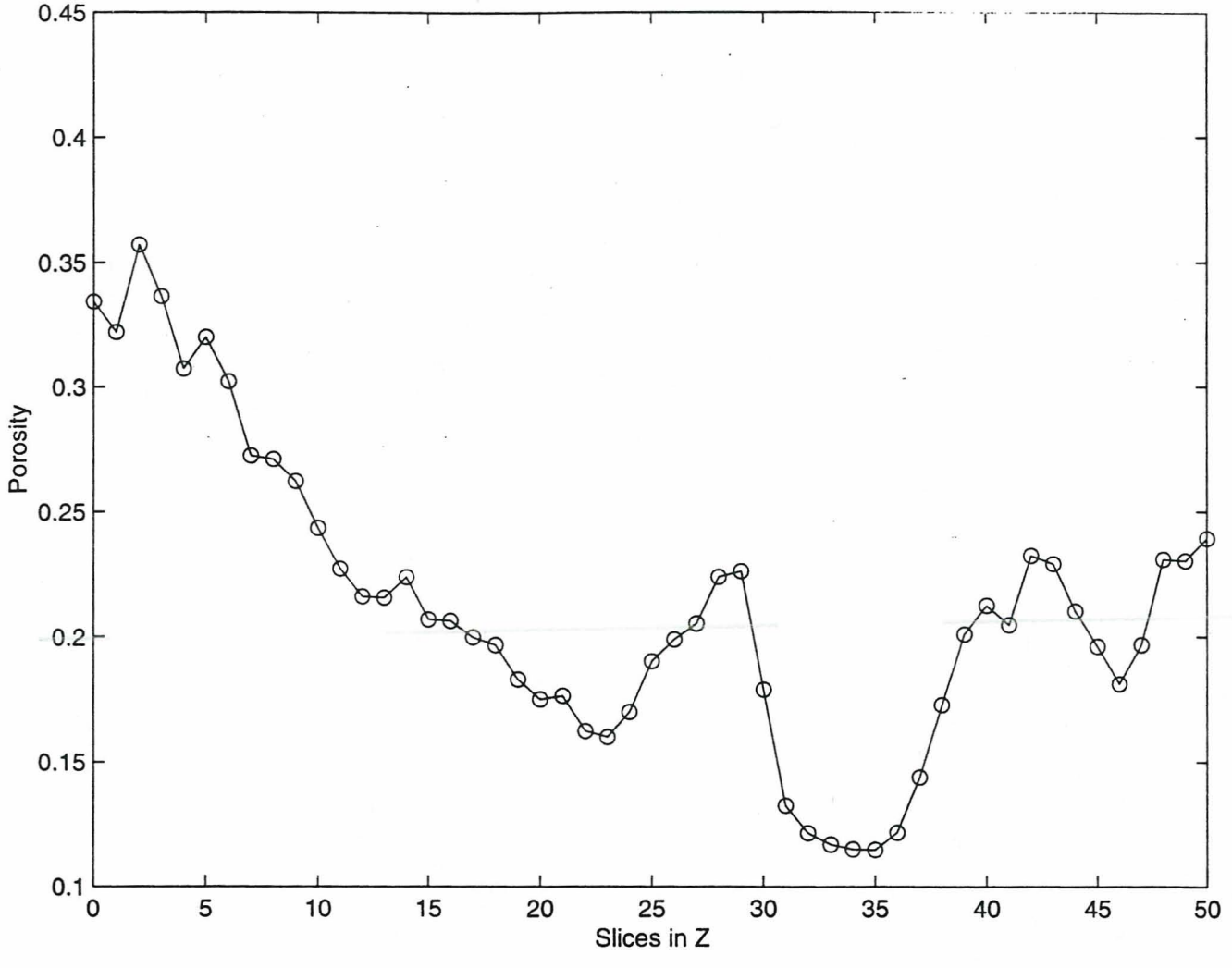

Figure 13: The porosity variations across the sample from slice 5 to 55.

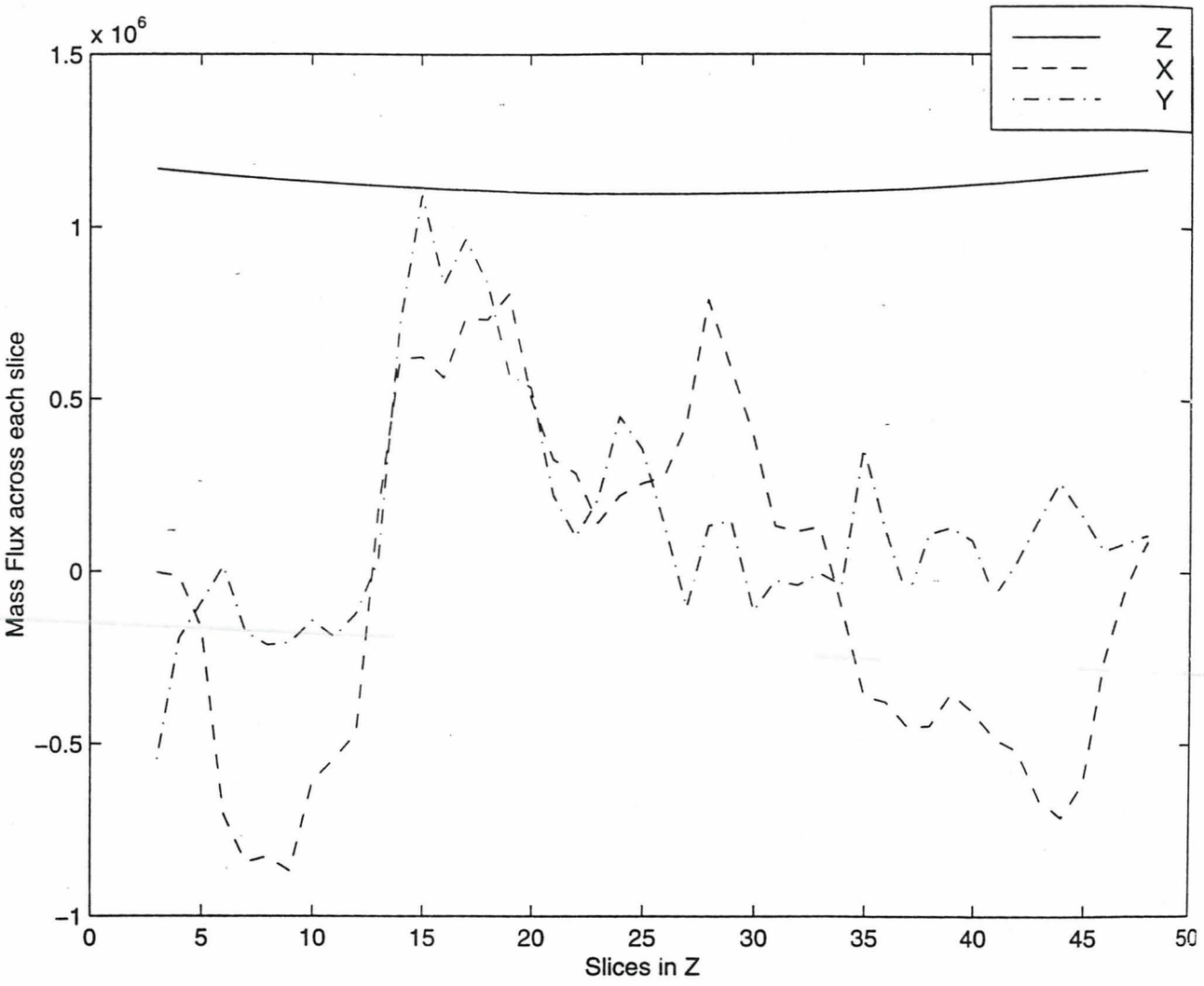

Figure 14: The mass flux plotted versus the slice through the rock. The Z flux is constant as expected.

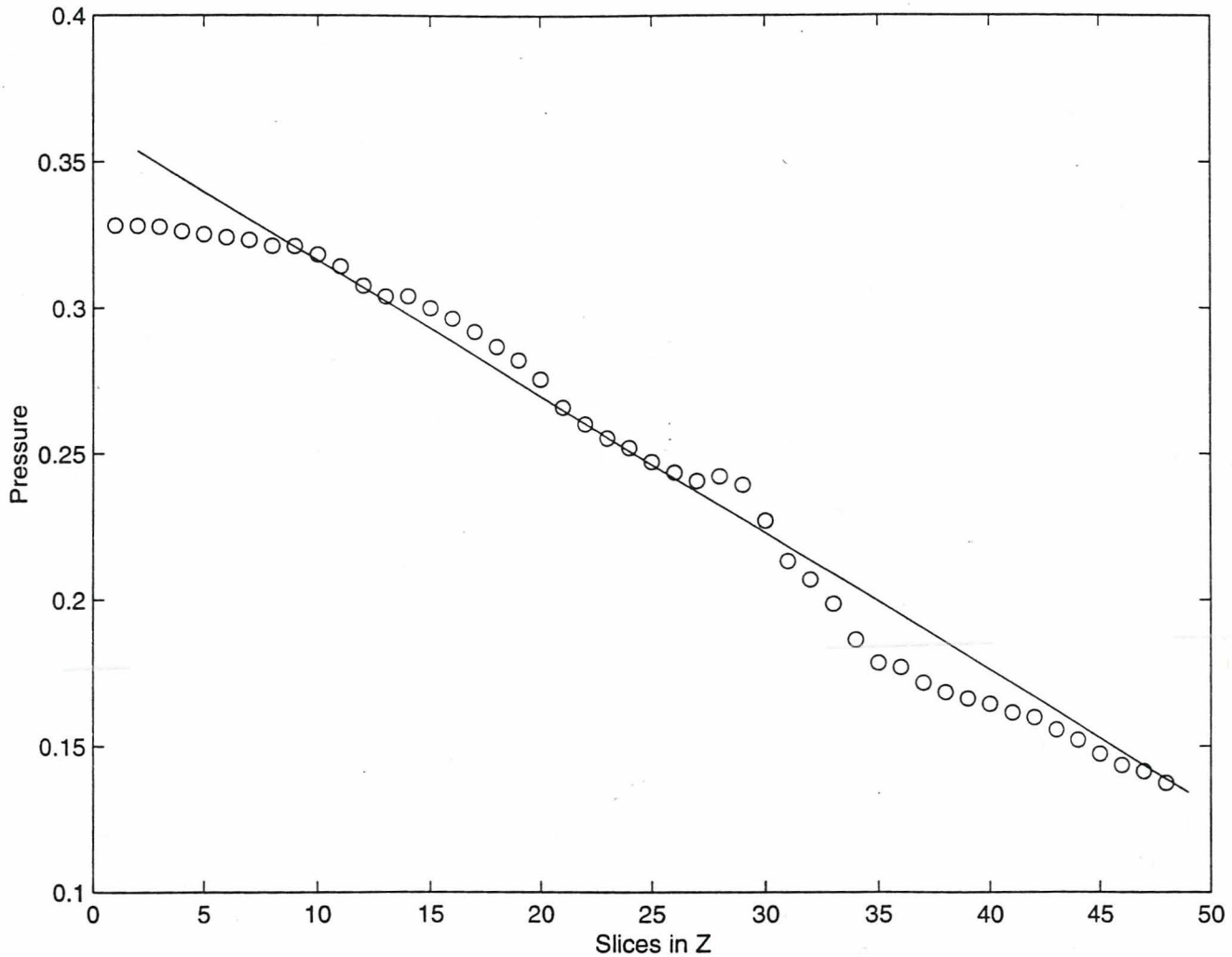

Figure 15: The pressure across the sample in the direction of the forcing.

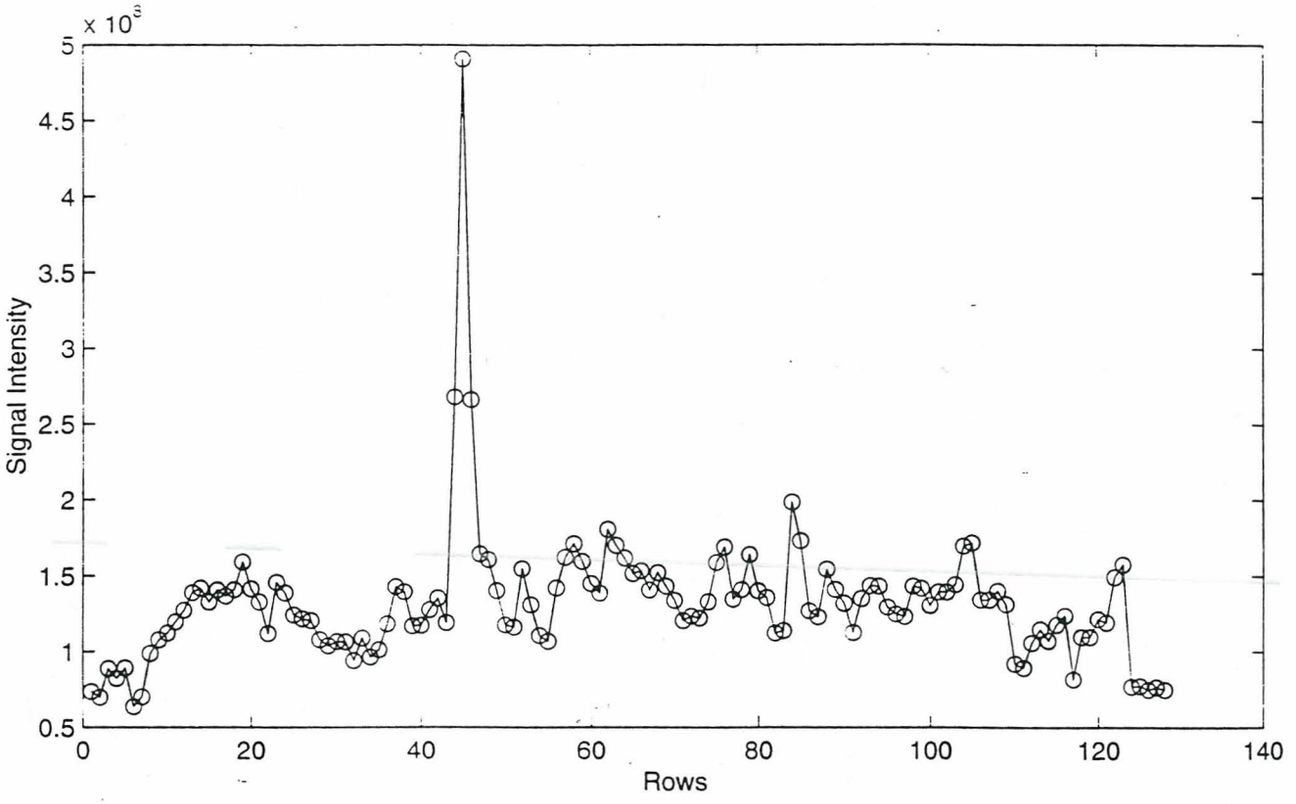

Figure 16: A plot of the maximum signal intensity for each row of slice 30. The peak at 45 is the bright spot seen in Figure 17. The noise and the signal are difficult to distinguish because of this peak.

Figure 17: The scaling effect from the bright spot at the center of slice 30. The light blue surrounding slice 30 is water and should have the same signal intensity as the red surrounding slice 20.

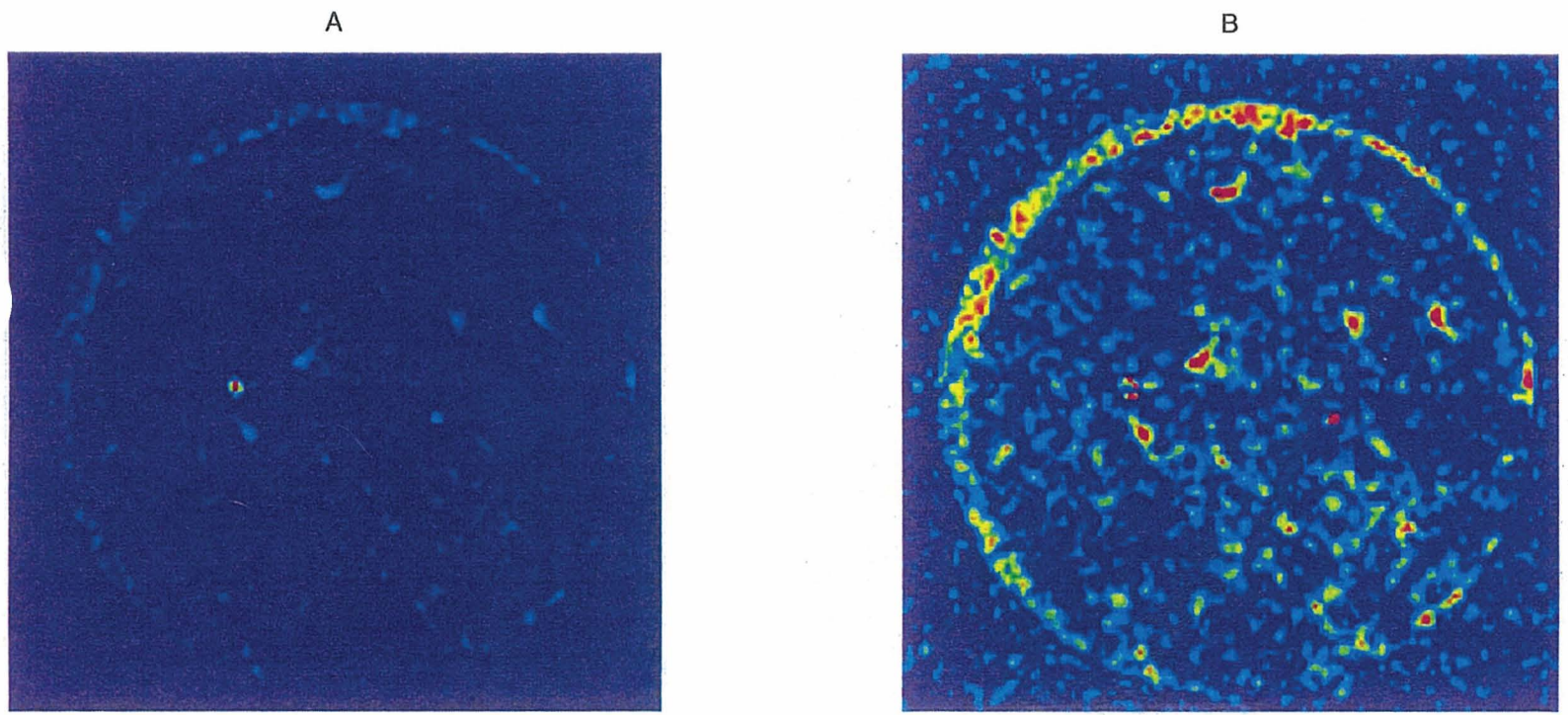

Figure 18: Slice 30 before rescaling (A) and after (B). The bright red spot was removed before scaling. The noise becomes larger after the scaling in the slices that have initially low signal intensity.